Journal of Organometallic Chemistry 904 (2019) 120999

Contents lists available at ScienceDirect

Journal of Organometallic Chemistry

journal homepage: www.elsevier.com/locate/jorganchem

Solvent free synthesis of ferrocene based rhodamine – hydrazone molecular probe with improved bioaccumulation for sensing and imaging applications

Smriti Dewangan [a], Tulasi Barik [a], Rakesh Parida [a], Shradha Mawatwal [b], Rohan Dhiman [b], Santanab Giri [c], Saurav Chatterjee [a, *]

[a] Department of Chemistry, National Institute of Technology Rourkela, Orissa, 769008, India
[b] Department of Life Science, National Institute of Technology Rourkela, Orissa, 769008, India
[c] Department of Applied Sciences, Haldia Institute of Technology, ICARE Complex, Haldia, 721657, W.B, India

ARTICLE INFO

Article history:
Received 16 August 2019
Received in revised form
11 September 2019
Accepted 22 October 2019
Available online 25 October 2019

Keywords:
Ferrocenyl
Hydrazone
Rhodamine
Sensor
Intracellular
Recognition

ABSTRACT

Functionalization of ferrocenyl hydrazone with rhodamine based tag using solid state synthetic method led to the formation of molecules containing both, fluorescent active and electroactive fragments, [(η^5-C_5H_5)Fe{(η^5-C_5H_4)C(R)=NNC(O)-X}] (R = CH_3, H; X = Rhodamine-6G). The molecules showed selective metal ion sensing and switching behavior with distinct interaction and influence from the organometallic fragment. The sensing behavior was explored within bacterial strain and THP-1 cancer cell lines to understand the subcellular distribution of heavy metal ions and their potential in applications related to bioimaging, uptake and bioremediation activities. The study showed significant intracellular metal recognition and bioaccumulation characteristics and understanding towards ferrocene based signaling behavior upon oxidation.

1. Introduction

Recently, considerable attention has been focused on the fabrication of devices in the molecular level for applications related to molecular electronics, bio-imaging, molecular machines, switching devices etc. [1] Integrating molecular compounds with photochromic functional moieties for the design of multifunctional photo-responsive materials have been widely used for their potential in several areas ranging from molecular optical switches, opto-electronic devices, logic gates to photo-biology [2,3]. Over the years, organometallic molecular systems have shown unique fluorescent properties and induced switching behavior using external stimuli which led to the development of fluorescence based sensors and molecular switches [3]. Among a range of organometallic species, ferrocenyl system plays a vital role as a remarkable redox signaling unit in various organometallic molecules or scaffold [4]. In addition, various functionalization of ferrocene with biologically active groups and their study on different biological properties led to the emergence of bio-organometallic chemistry, where a large number of organometallic based compounds have been found to display interesting biological activities [5]. Rhodamine dye based fluorescent component has been used recently to construct "off-on" type fluorescent chemosensors because of its exclusive structural identity having a xanthene moiety which can be strategically functionalized to form a heterocyclic spirolactam type ring system attached to the xanthene ring via a carbon atom [6]. Spirolactam frameworks are usually non-fluorescent, whereas ring opening of the spirolactam gives rise to a strong fluorescent emission band. As a part of our ongoing interest in using sandwich and half-sandwich organometallic fragments for sensor based application and photo-induced behavior [7–9,19,20], we focused our study on rhodamine based sandwich organometallic moieties and exploit their fluorescence and sensing behavior. We envisioned that the presence of an electroactive fragment and a highly emissive rhodamine based photo-responsive component into a molecular compartment may create a fluorescent single molecule - probe for applications related to sensor and switching type molecular devices.

Heavy metal ion toxicity has been widely studied across various

* Corresponding author.
E-mail address: saurav@nitrkl.ac.in (S. Chatterjee).

https://doi.org/10.1016/j.jorganchem.2019.120999
0022-328X/

biological systems and are known to cause severe damage to virtually all organs affecting mainly the central nervous system. Recently, biological remediation technologies have been largely studied in which microorganisms play a vital role in metal adsorption, intracellular accumulation and bioremediation techniques [10]. However, the mechanism by which these biological systems are involved in the uptake of selective metal ions and their detoxification is very complex and are under part of extensive research study worldwide [11]. Several bacterial species are known to form biofilm, which are organized group of cells clumped together within a self-produced hydrated matrix or EPS and triggers bioremediation of heavy metal ions with pronounced metal binding and complexation potential [12]. Therefore, a convenient and facile method for visualizing the concentration and subcellular distribution of heavy metal ions in biological samples has an important consequence in several biological studies. Conventional methods use AAS and ICPMS, which are highly expensive instruments and requires tedious analytic methods to be used in effective detection of heavy metal ions like Hg^{2+} in biological samples [13]. In contrast, fluorescent bioimaging technique with suitable molecular scaffold has been very effective and provides systematic analysis of metal ions without cell damage [14]. But, the design of such molecular sensors for sensitive and selective detection of environmentally and biologically important ionic species has been a challenge due to the poor accumulation of the receptor in the intracellular matrix. Thus, it is very important to design effective and benign sensors for the in-vitro detection of Hg^{2+} with sufficiently high bioaccumulation of the receptor in the cellular environment. We have, recently, explored the use of organometallic scaffold attached to fluorescent active moieties to study the selective interaction of Hg^{2+} and Pb^{2+} ions and their capacity for sensing inside bacterial and cancer cell lines [7a,7c]. To understand the potential of various other organometallic fragments as receptor unit and to focus our study on the selective interaction with heavy metal ions and imaging within intracellular matrix, we have described in this report, the synthesis of fluorescent active ferrocenyl hydrazone compounds and observed their distinctive sensing and redox based switching properties. However, to achieve such molecular system we chose to use a novel solid state reaction method that can provide mild reaction condition, easy separation procedure and increased yield. Inorganic support plays an important role in chemical synthesis and also attracted much attention due to their ability to perform difficult reactions [15,16]. Solid state, solvent free reactions using organic substrates are widely used for improved product synthesis, while solid supported reactions involving organometallic fragments have been rarely studied [17,18]. As a part of our study to understand the wider scope of solid supported reaction, we recently identified Rice Husk Silica (RHA) as a remarkable solid support for the synthesis of bioactive bifunctionalized unsymmetrical ferrocenyl compounds [19,20]. In the present study, we have chosen Rice husk ash (RHA) as solid support due its high silica content and wide availability, to prepare different ferrocene linked rhodamine hydrazone and explored their metal interaction and redox signaling property. We have also explored the sensing behavior inside bacterial and cancer cell lines to understand their bioaccumulation capabilities for applications related to bio-imaging, uptake and bioremediation activities. To our knowledge ferrocenyl - hydrazone compounds have never been explored for the study associated to intracellular imaging and detection of Hg^{2+} ion both in bacterial and cancer cell lines. Surprisingly, the first article for the use of Hg(II) sensitive fluorescent probe for the imaging in both cancer cell and bacterial cell has been recently reported by Pan et al. [21] using an organic compound, and soon after, we had reported Hg^{2+} detection using an organometallic half-sandwich based probe for cancer cell and bacterial cell imaging [9a]. Herein, we report the synthesis of another class of organometallic based fluorescence probe to understand their metal ion interaction capabilities and their imaging behavior within cancer cell lines and in bacterial species. We have also described the electrochemical properties and their potential in oxidative switching behavior for signaling related application.

2. Results and discussion

Ferrocenyl molecules are ideal system to act as a remarkable redox signaling unit, while rhodamine fragments are well known fluorescent active models for various photo-responsive activities. To achieve such molecular system containing both rhodamine and ferrocenyl moieties, reactions was carried out with mono-acetylferrocene or mono-carboxaldehyde ferrocene and rhodamine-6G-hydrazides under solvent free reaction condition using rice husk ash (RHA) as solid support to obtain ferrocenyl rhodamine hydrazone, [{(η^5-C_5H_5)Fe(η^5-C_5H_4)C(R)═NNC(O)-X}] in high yields (Scheme 1) (R = CH_3 (**1**), H (**2**); X = Rhodamine-6G). The compounds were isolated and purified using preparative TLC for spectroscopic characterization. Attempts to synthesize compounds **1** using solution based acid catalyzed reaction method were not facile as it gave very low yield of the product with increased decomposition and impurity. In comparison, the solid state reaction using rice husk ash gave remarkable yields for compounds **1** and **2** with better selectivity and easy isolation process without any decomposition. Recently, solution based synthesis of compound **2** has been reported by Wu et al. which showed metal sensing property.[4(d)] However, the intracellular imaging and metal detection was not evaluated. Interestingly, the synthesis of compound **1** and its metal sensing behavior, both extracellularly and intracellularly, has remain unexplored as per our knowledge. Therefore, we explored the synthesis of both **1** and **2** using our solid state method to understand their metal sensing behavior inside different biological medium.

Compounds **1** and **2** were characterized by infrared, ^{1}H, ^{13}C NMR and mass spectrometric analysis. Infrared spectra for compounds **1** and **2** reveal the presence of ketonic groups in the region 1708 - 1682 cm^{-1} and peaks corresponding to −C═N has been detected in the region 1637 - 1607 cm^{-1}. ^{1}H NMR spectra of **1** and **2** show the presence of protons corresponding to ferrocene based unsubstituted cyclopentadienyl group at δ 3.94 (singlet) and δ 3.81 (singlet) regions, while substituted cyclopentadienyl peaks have been found at δ 4.24 (triplet), δ 4.51 (triplet) and δ 4.23 (triplet), δ 4.51 (triplet) regions respectively. Methyl protons for compound **1** was observed at δ 1.95 and δ 2.07 region due to rhodamine based and imine based methyl groups respectively. In contrast, compound **2** shows the presence of only one peak in that region (δ 1.91) corresponding to the methyl groups attached to xanthene ring. A triplet and a quartet peak at δ 1.30 (**1**), 1.34 (**2**) and δ 3.20 (**1**), 3.24 (**2**) respectively have been observed corresponding to the ethyl protons present in both the molecules. In addition, aromatic protons for **1** and **2** are observed at δ 6.39 - δ 8.00 and δ 6.42 − δ 8.08 regions respectively (Figs. S1 and S4). ^{13}C NMR spectra for both the compounds (**1**, **2**) showed peaks corresponding to methyl carbon from δ 14.07 to δ 38.73 regions while cyclopentadienyl carbons at δ 67.99, δ 69.06, δ 70.01, δ 79.14 regions and δ 68.21, δ69.54, δ 70.21 and δ 81.63 for compounds **1** and **2** respectively. Aromatic carbons have been observed at δ 96.69 - δ160.25 regions, while peaks at δ 152.37 and δ 160.25 may be assigned to −C═N for **1** and **2** respectively. Ketonic carbon peak was found at δ 164.66 and δ 172.06 for **1** and **2** respectively (Figs. S2 and S5). Mass spectral analysis for **1** and **2** showed the characteristic molecular ion peak, $[M+1]^+$ at *m*/*z* 639.56 and 625.36 respectively.

Absorption spectral data of **1** shows the presence of very weak

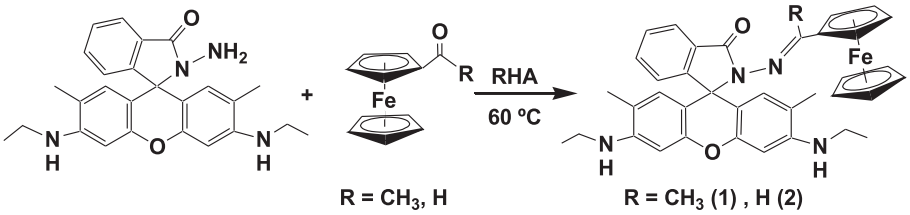

Scheme 1. Synthesis of **1** and **2** (RHA: Rice husk ash).

lower energy bands at 523 nm and 491 nm regions, while moderate to strong intensity bands were observed at high energy regions at 341 nm, 302 nm, 260 nm and 230 nm regions. Compound **2** also shows similar pattern bands at 551 nm, 351 nm, 310 nm and 274 nm regions. Fluorescence spectroscopic analysis of **1** reveals that on excitation at 510 nm region, the compound shows very weak intensity emission band at 541 nm region. The weak fluorescence has been predicted due to the formation of five membered spirolactam ring in compound **1**. Compound **2** also shows weak emission spectra at 543 nm on excitation at 500 nm wavelength due to similar reason.

Our previous report reveals that spirolactam rings are usually colorless and non-fluorescent but are very much susceptible to acidic species and are known to break in presence of H^+ ion and selected metal ions [9] resulting in the change in solution color and observation of strong fluorescence response. We anticipated that metal ion recognition behavior for this system might also be interesting and could lead to new observations where the organometallic fragment may have some influence on the binding property. Thus, a series of metal perchlorate salts, Na^+, K^+, Mg^{2+}, Ca^{2+}, Ba^{2+}, Mn^{2+}, Ni^{2+}, Co^{2+}, Cd^{2+}, Zn^{2+}, Fe^{2+}, Pb^{2+}, Cu^{2+}, Al^{3+} Ag^+ and Hg^{2+} were used to study the metal ion recognition behavior of compounds **1** and **2**. The UV–Visible absorption studies have been performed using a C_2H_5OH/PBS buffer (2:8, v/v, pH 7.4) solution. The UV–Visible spectra of **1** and **2** showed absorption maxima in the range of 210 nm–320 nm due to intramolecular $\pi-\pi^*$ charge transfer transitions. No absorption peak was observed in the visible wavelength region above 400 nm, which indicates that both the receptors exist in a spirocyclic form in solution. The UV–Visible spectral based metal binding properties of **1**, **2** were examined through a titration experiment using different metal perchlorate salts. With the addition of Hg^{2+}, a new absorption peak emerged at 528 nm and 531 nm, for compounds **1** and **2** respectively which was in accordance with the typical absorption wavelength of ring-open form of the attached rhodamine group. The intensity of absorption increased along with the increasing concentration of Hg^{2+} in a good linear relationship (Figs. S10 and S11). Highly selective Hg^{2+} recognition behavior has been observed for compound **1**, while for compounds **2**, Pb^{2+} also showed slight increase in absorption intensity whereas the other metal ions like Na^+, K^+, Mg^{2+}, Ca^{2+}, Ba^{2+}, Mn^{2+}, Ni^{2+}, Co^{2+}, Cd^{2+} and Zn^{2+} showed insignificant response in the absorption peak for both the receptors (Figs. S7 and S8). The quantum yield (ϕ_f) determination revealed the increase in ϕ_f from 0.003 for the free receptor **2** to that of 0.35 for the Hg^{2+} interacted solution, while the quantum yield for the free receptor **1** is 0.007 which changes to that of 0.4 on addition of Hg^{2+} in solution. Additionally, the ratio-relationship between [**2**.Hg^{2+}] and [**1**.Hg^{2+}] was estimated with a Job's plot experiment as shown in Fig. S9. The maximum value of the absorption appeared at 0.5 mol fraction, which indicated that the stoichiometry of the **1**/Hg^{2+} and **2**/Hg^{2+} complex was 1:1. The intensity of absorption increased along with the increasing concentration of Hg^{2+} in a good linear relationship ($R^2 = 0.978$ and 0.994) (Fig. S10). According to the UV–Visible titration experiment, the graph of **1**/$(A - A_0)$ versus **1**/[Hg^{2+}] at 543 nm holds a good linear relationship with $R^2 = 0.989$. Similarly, **2**/(A -A_0) versus **2**/[Hg^{2+}] at 542 nm showed $R^2 = 0.988$ with a linear graph (Fig. S11), consistent with the Job's plot result.

The weak fluorescent emission for compounds **1** and **2** centered at 541 nm and 543 nm respectively shows highly selective increase in the intensity of the emission peak with a distinct red shift of around 14–16 nm on gradual addition of Hg^{2+} cation to the buffer solution of **1** and **2**. The other metal ions like Na^+, K^+, Mg^{2+}, Ca^{2+}, Ba^{2+}, Mn^{2+}, Ni^{2+}, Co^{2+}, Cd^{2+}, Zn^{2+}, Fe^{2+}, Al^{3+} and Pb^{2+} showed insignificant response with receptor **1**, while receptor **2** showed little increase in the emission peak on gradual addition of Pb^{2+} (Figs. 1 and 2). This reveals that the methyl analogue (**1**) is highly selective for Hg^{2+} interaction in comparison to receptor **2**.

Furthermore, the color of the solution of **1** and **2** changed significantly after interaction with Hg^{2+} from colorless to pink by naked-eye observations. We propose that the sharp increase in the emission peak for the receptors **1** and **2** by addition of respective metal ions is because of a ring-opening process at the spirolactam moiety mediated by metal cations. Highly selective recognition behavior has been observed with compound **1** while, non-selective response was observed with compound **2.** This is possibly due to the difference in the substitutional variation of the group attached to the imine carbon, which may affect the overall interaction of the metal ion inside the receptor pocket.

The values of fluorescence intensity were proportional to the concentration of Hg^{2+} with a good linear relationship ($R^2 = 0.989$ and 0.990) (Fig. 1(b)). The fluorescence turn-on response of **1** and **2** was in good agreement with the results of the UV–Visible titration studies, which demonstrated that this receptor was a qualitative and quantitative chemosensor for Hg^{2+}. The reversibility of the sensing process between **1**, **2** and Hg^{2+} was examined by the addition of EDTA into the interacted solution. The spectral data revealed that addition of 1 equivalent of EDTA to [**1**.Hg^{2+}] and [**2**.Hg^{2+}] systems could restore the "ON" state back to the "OFF" state in both absorption and fluorescence spectral signals (Fig. 3). Moreover, adding extra Hg^{2+} to the system could once again turn on the signals, which proved the sensing processes reversible. Considering the spectral changes investigated above and the 1:1 binding stoichiometry confirmed by the Job's plot, the sensing mechanism between **1**, **2** and Hg^{2+} could be speculated that the Hg^{2+} ion is going inside the receptor pocket and interacting with the ketonic oxygen and imine nitrogen resulting in the rupture of five membered spirolactam ring. The opening of the five membered ring led to a color change and a strong fluorescence emission peak was observed.

Thus, the Hg^{2+} interaction gave rise to dual signaling process by the change in their color and fluorescence behavior. The mode of binding was supported by solid infrared spectroscopy which showed a distinct shift of the –C=O stretching frequency from 1700 cm^{-1} to 1690 cm^{-1} on addition of Hg^{2+}. The formation of 1:1 (cation/receptor) stoichiometry was also confirmed by Job's plot which shows maxima at 0.5 mol fraction.

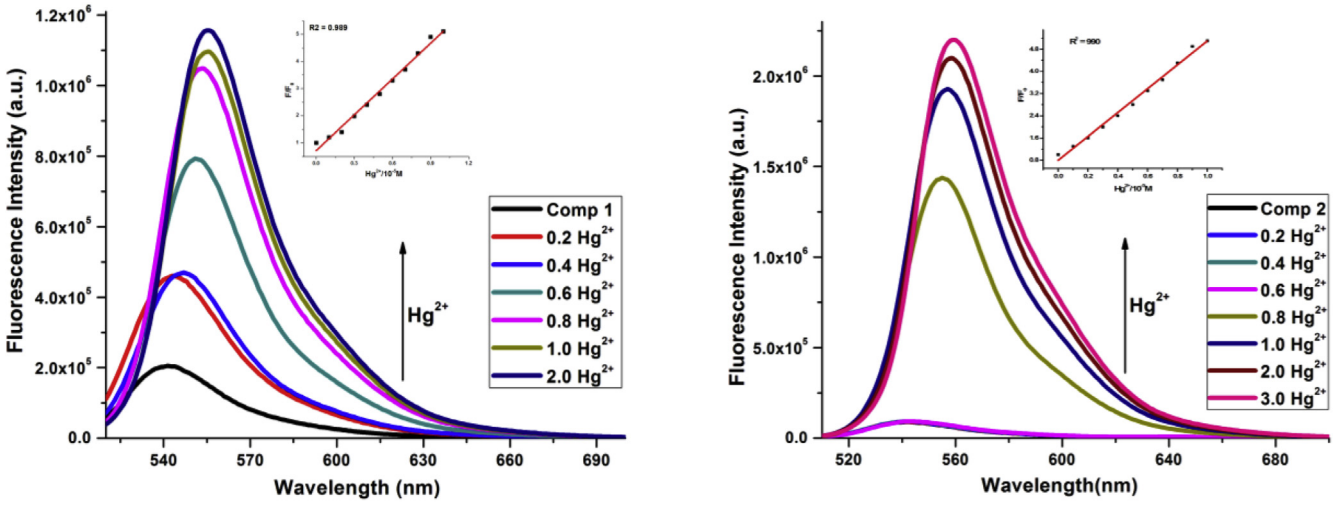

Fig. 1. (a) Fluorescence response of **1** and **2** upon addition of Hg^{2+}. (b) Inset: Linear relationship of fluorescence intensity with Hg^{2+} concentration.

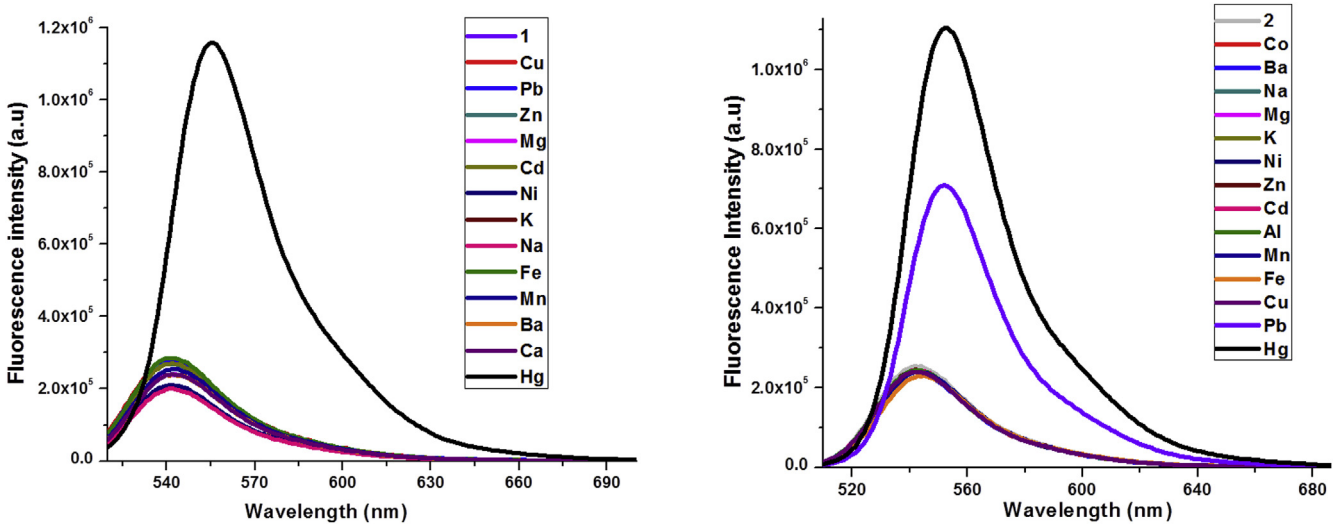

Fig. 2. Fluorescence emission spectra of compounds **1** and **2** with different metal ions.

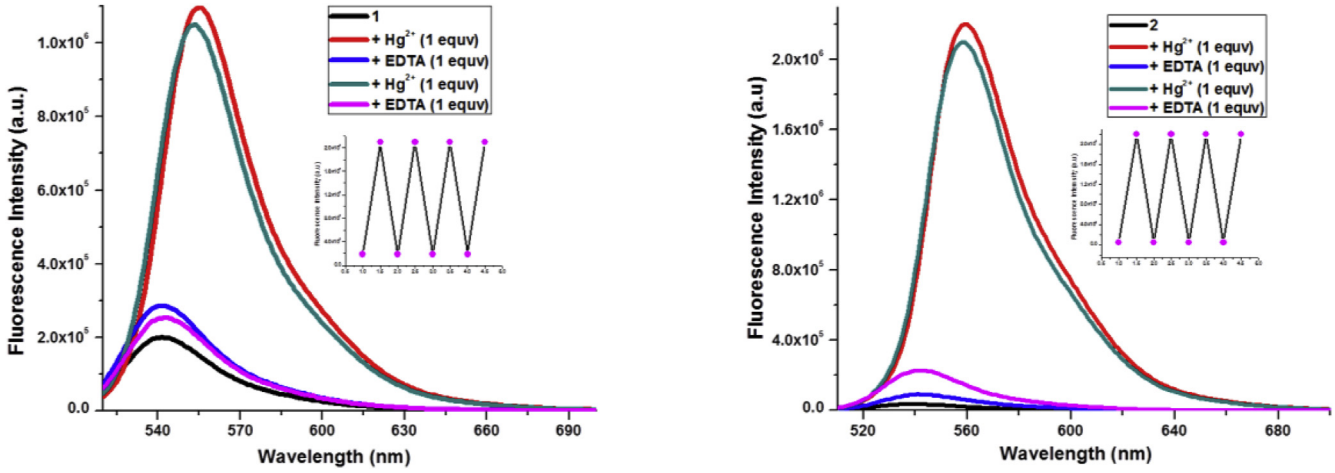

Fig. 3. Reversibility graph of compounds **1** and **2** by adding Hg^{2+} and EDTA.

In order to confirm the mode of interaction, geometry optimization and DFT calculations was carried out for the free receptors, (**1**, **2**) and their respective Hg^{2+} complexes, [**1**.Hg^{2+}] and [**2**.Hg^{2+}]. The optimization for all the systems was done using LANL2DZ basis set at B3LYP level. On the basis of experimental observations like absorption, emission, and cyclic voltammetric studies the binding ratio of the complexes was found to be 1:1. Therefore, the mononuclear complexes, [**1**.Hg^{2+}] and [**2**.Hg^{2+}], involving 1:1 interaction between the receptor and Hg^{2+} were optimized by DFT calculations. The optimized structures have been depicted in Fig. S14 and Fig. S15, which reveal that both the free receptors (**1**, **2**) contain a ferrocene based rhodamine hydrazone unit with the presence of a five membered spirolactam ring. In contrast, [**1**.Hg^{2+}] and [**2**.Hg^{2+}] shows the presence of Hg atom strongly bonded to an imine nitrogen ($d_{Hg-N} = 2.332$ Å, 2.343 Å) and a ketonic oxygen atom ($d_{Hg-O} = 2.279$ Å, 2.291 Å) and the absence of the five membered spirolactam ring. Interestingly, the Hg ion has also been found to strongly interact with the ferrocenyl iron and cyclopentadienyl carbon atoms ($d_{Hg-Fe} = 2.836$ Å, 2.840 Å; $d_{Hg-C} = 2.618$ Å, 2.621 Å) for both the complexes, [**1**.Hg^{2+}] and [**2**.Hg^{2+}] resulting in slight tilting of the ferrocenyl rings from planarity as shown in Scheme 2. In addition, the ketonic bond has been markedly elongated from 1.256 Å and 1.258 Å to $d_{C-O} = 1.328$ Å and $d_{C-O} = 1.323$ Å for [**1**.Hg^{2+}] and [**2**.Hg^{2+}] respectively. The tilting of cyclopentadienyl rings in ferrocene is very rare and has been recently observed in a structurally characterized ferrocenyl hydride, where the space between the two cyclopentadienyl rings opens up to accommodate a hydride ligand [22]. In a similar fashion, [**1**.Hg^{2+}] and [**2**.Hg^{2+}] also results in the opening of a space by the tilting of cyclopentadienyl rings for the accommodation of Hg^{2+} cation and interaction with the iron center.

Orbital energies of the highest occupied molecular orbital (HOMO) and the lowest unoccupied molecular orbital (LUMO) and the electronic distribution of [**1**.Hg^{2+}] and [**2**.Hg^{2+}] have been shown in Fig. 4. The HOMO of both the free receptors **1** and **2** are mostly located on ferrocenyl fragment, while the LUMO is primarily located on the spirolactam ring which supports the fluorescence quenching. In the complex, [**1**.Hg^{2+}], the HOMO, HOMO-1 and HOMO-2 is spread over the ferrocene, hydrazone linkage and Hg atom and the HOMO-3 is mainly located on the xanthene fragment. The HOMO and HOMO-1 for complex [**2**.Hg^{2+}] are concentrated on xanthene moiety while HOMO-2 and HOMO-3 are delocalized across the whole molecule. LUMO's of both the complexes are also found to be spread over whole molecule (Table S2). The strong absorbance at around 530 nm due to the interaction with Hg^{2+} has been assigned mainly for the transitions from HOMO-3 to LUMO in [**1**.Hg^{2+}] and HOMO to LUMO+2 in [**2**.Hg^{2+}]. The calculated data also indicated that on binding of Hg^{2+} with **1** and **2** the HOMO−LUMO energy gap of the complex decreases thereby stabilizing the system, which correlates with the observed red shift in the fluorescence and absorption spectra.

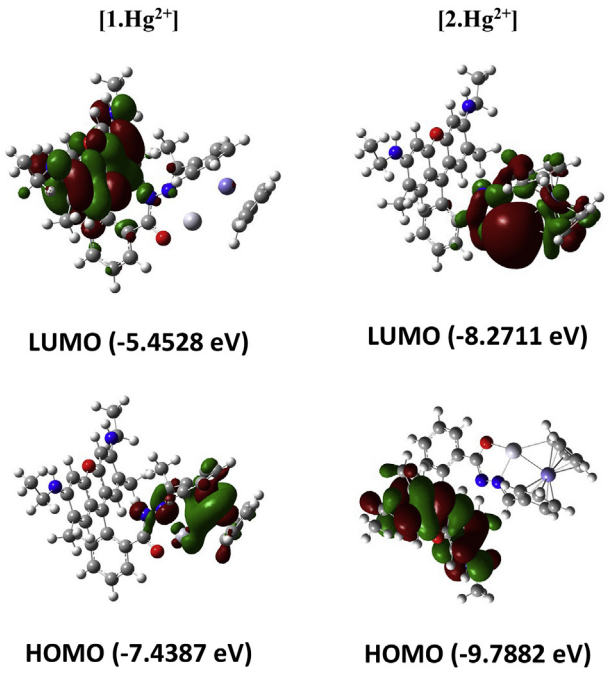

Fig. 4. HOMO and LUMO of [**1**.Hg^{2+}] and [**2**.Hg^{2+}].

The electrochemical properties of **1** and **2** were examined in acetonitrile solution [0.1 M tetrabutylammonium perchlorate (TBAP)] by cyclic voltammetry and differential pulse voltammetry (DPV). Both the compounds **1, 2** containing a ferrocenyl moiety linked to a hydrazone group, exhibited one reversible redox process between +0.41 and + 0.42 V owing to the FeII/FeIII redox couple (Fig. 5)**.** In addition, one irreversible anodic peak has also been observed in between +0.8 V and +0.9 V due to the presence of amide linkage in the spirolactam-rhodamine moiety (Table 1). All the electrochemical potentials were recorded vs SCE in which the ferrocene/ferrocenium redox couple (Fc/Fc^{+}) was observed at + 0.37 V.

As a part of our interest in electrochemical signaling applications and to further understand their potential as sensor based system, we carried out systematic cyclic voltammetric analysis of compounds **1** and **2** by gradual addition of Hg^{2+} ion. The recorded spectral data showed that on gradual addition of the metal ion, the reversible redox anodic peak shifted to a more positive potential, while the redox peak at +0.84 V (**1**) and +0.9 V (**2**) shifted sharply and disappears due to the breaking of the spiro ring (Fig. 6, Fig. 7). The color of the solution gradually turned pink during the

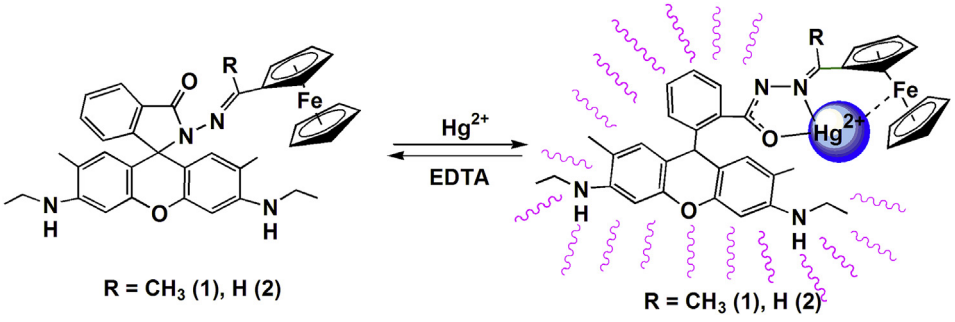

Scheme 2. Interaction of Hg^{2+} with receptors **1** and **2**.

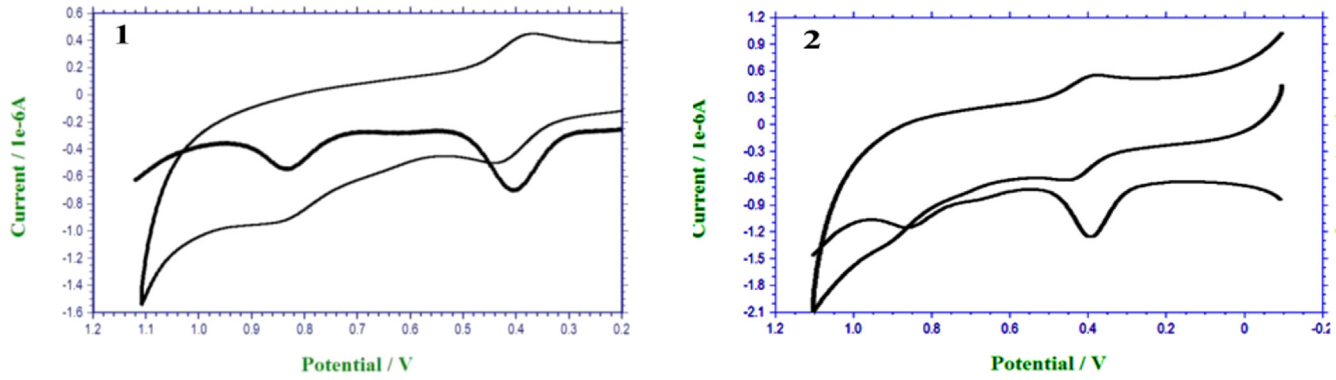

Fig. 5. Cyclic voltammogram and Differential Pulse Voltammetry of **1** and **2**.

Table 1
Cyclic voltammetry and Differential pulse voltammetric data.

Compounds	Ep_a(V)	Ep_c(V)	$E_{1/2}$ (V)(ΔE (mV))	dpv (V)
1	0.43, 0.84	0.38,–	0.41 (50)	0.40, 0.83
2	0.44, 0.9	0.40,–	0.42 (40)	0.39, 0.87

*In acetonitrile at a scan rate of 50 mv s^{-1}. $E_{1/2}$ (V) = (E_{pa} + E_{pc})/2, where E_{pa} and E_{pc}arethe anodic and cathodic peak potentials respectively. ΔE_p (mV) = E_{pa}-E_{pc}.

electrochemical experiment. Cyclic voltammetric titration of compound **2** was also carried out with Pb^{2+} ion, but the resulting anodic peak shifting is not significant which revealed that the binding with Pb^{2+} is not strong enough to produce a detectable electrochemical signal (Fig. S13).

Superior metal binding activity and the exciting redox based signaling properties of compounds **1** and **2** prompted us to understand their underlying electron transfer behavior, particularly on oxidation of the attached ferrocenyl moiety. Ferrocenyl component being an electroactive species, the reversible oxidation of the ferrocene entity may substantially influence the molecular

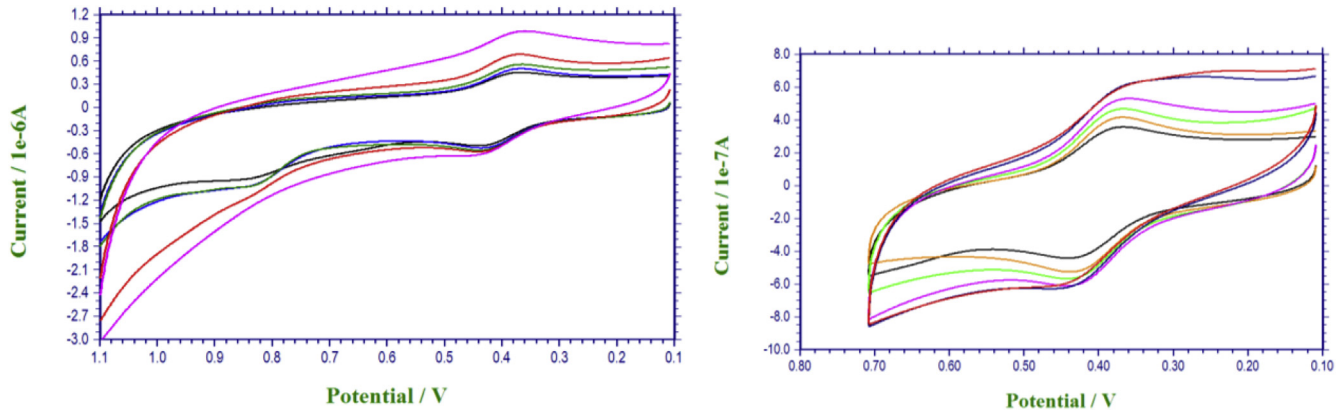

Fig. 6. CV of **1** (black) (10^{-5} M) on addition of Hg^{2+}.

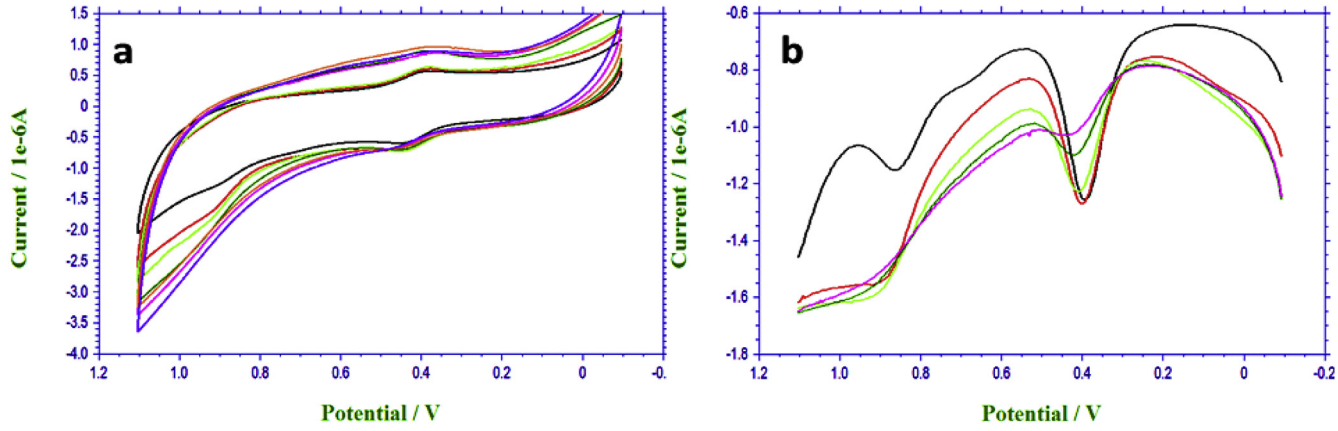

Fig. 7. (a) CV and (b) DPV of **2** (black) (10^{-5} M) in CH_3CN solvent on addition of Hg^{2+}.

property and trigger some useful electronic processes. In this regard, a lot of biological processes are documented where ferrocene oxidation plays a vital role in cell inhibition. Early literature shows that ferrocene is non-toxic to cancer cell lines whereas ferrocenium are highly toxic. Similarly, ferrocifens are well documented molecules which are found to be activated by in situ oxidation to form a cytotoxic quinone methide species [5b,5d–5h].

Moreover, the biological potential has been found to be sufficient to oxidize the ferrocenyl system and act accordingly. This prompted us to focus our study to understand the use of attached ferrocenyl moiety as an electroactive agent to modulate the whole molecular system and subsequently influence the electronic property of the rhodamine ring at the other end of the molecule. Our experimental observation reveals that on gradual oxidation of ferrocene to ferrocenium ion coulometrically, compound **1** triggers unusual increase in the fluorescence intensity as shown in Fig. 8. The increase in the fluorescence intensity is very similar to that of when Hg^{2+} binding prompted the disruption of the spirolactam ring of the rhodamine moiety. The oxidation process also led to the change in the UV–Visible absorption peaks and color of the solution from colourless to pink. On oxidation of ferrocenyl component a new peak at 520 nm region is generated in the UV–Visible spectrum (Fig. S12). On the basis of this analogous behavior we proposed an electron transfer mechanism in which on oxidation the ferrocenyl fragment generates a ferrocenium species which triggers interaction of the ketonic oxygen and imine nitrogen atoms with the ferrocenyl iron center leading to the breakage of N–C bond and disruption of the five membered spirolactam ring as shown in Fig. 9.

The proposed mechanism has been confirmed by DFT study of compound **1** and its oxidized species $\mathbf{1}^{+}$. DFT calculations were performed using LANL2DZ basis set at B3LYP level on the fully optimized structures of the compound (**1**) and its oxidized species ($\mathbf{1}^{+}$) in gas phase. The optimized geometry of $\mathbf{1}^{+}$, shown in Fig. 10, reveals distinct interaction of the ketonic oxygen and the imine nitrogen atoms of the hydrazone chain with the iron center (Fe(III)) of the ferrocenyl moiety and the rupture of the five membered spirolactam ring. Shortening of the non-bonding distances between Fe and O(ketonic) and between Fe and N(imine) has also been observed, while lengthening of the ketonic C–O bond from 1.256 Å to 1.328 Å has been detected. In addition, the two cyclopentadienyl rings have been observed to be slightly tilted against each other with an angle of 19.2°, possibly due to the Fe···O and Fe···N interactions in the oxidized species, $\mathbf{1}^{+}$.

NBO population analysis was performed on **1** and its $1e^{-}$-oxidized species, $\mathbf{1}^{+}$ to understand electron population at the iron center. The natural electron spin population ($\alpha-\beta$) at the iron atom in $\mathbf{1}^{+}$ species has been found to be 0.89468 which indicates that during oxidation, one electron is released mainly from the ferrocenyl iron center (Table S1).

Selective binding of **1** and **2** with heavy metal ions like Hg^{2+} prompted us to study their potential in applications related to fluorescence imaging inside bacterial and cancerous cells. Sensing and uptake of metal ions by bacterial cells using their unique biosorption ability have been well known [23], but the complexity by which these prokaryotes interact with metal ions and act during infection are poorly understood and under investigation by various groups. However, bacterial cells have a unique technique to uptake metal ions from waste and other sources with a control in the concentration of the metal ion biosorption [24]. These metal ions are also essential for microbial pathogens during infection, as they are involved in bacterial metabolism and various virulence factor functions [25]. In view of the huge implications of metal ion interactions inside the bacterial cell we initiated our study on the use of compound **1** as a bioimaging agent during metal ion interaction within the bacterial cell. The fact that compound **1** on interaction with Hg^{2+} ions gave rise to fluorescent ON type system along with the compound's non-toxic behavior towards bacterial cells, prompted us to study bioimaging experiment using compound **1** with and without metal ion. We have used *E. coli* bacterial strain and Hg^{2+} metal ion for the bioimaging investigation using Confocal Scanning Laser Microscopic study. The bacterial cells were first

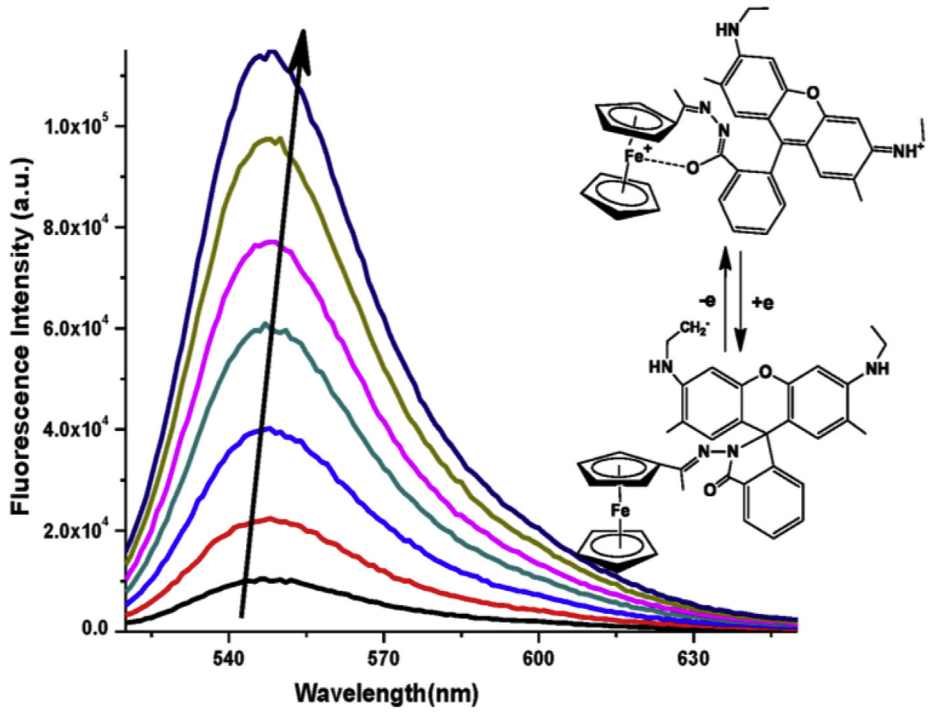

Fig. 8. Fluorescence emission spectra of compound **1** on oxidation (5×10^{-6} M).

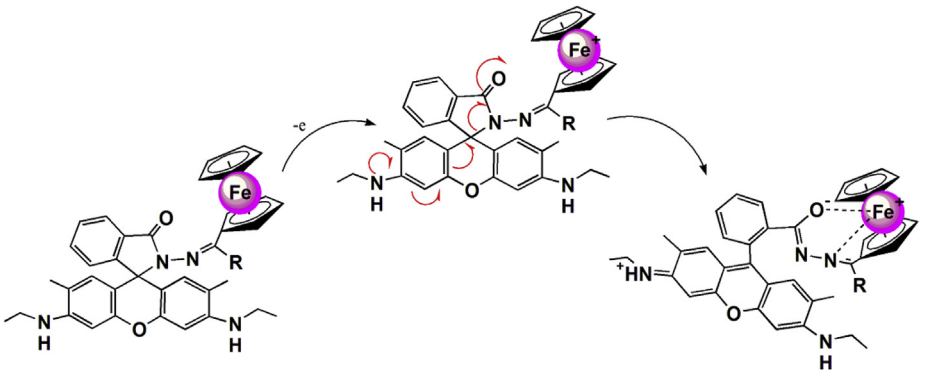

Fig. 9. Ferrocenyl oxidation and interaction.

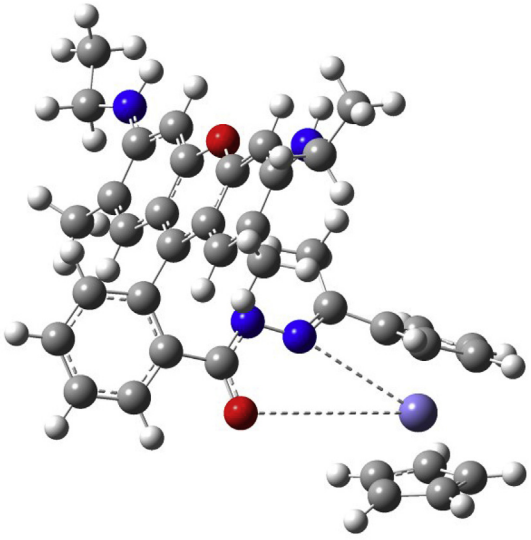

Fig. 10. Optimized structure of **[1^{+}]** oxidized species.

treated with compound **1** and then Hg^{2+} metal cation was added to the bacterial culture in different concentrations ranging from 1 ppm to 100 ppm level. Imaging using confocal fluorescence microscopy using red channel indeed revealed distinct increase in fluorescence intensity of the bacterial cells with increasing concentration of the metal ions as shown in Fig. 11. It is evident that the compound can able to penetrate the bacterial cell wall without any damage and can be used for imaging applications. A plot between the raw integrated density of the bacterial cell fluorescence and the concentration of Hg^{2+} confirms more than 30 times increase in the density as the concentration was varied from 0 ppm to 100 ppm (Fig. S16).

2.1. Cancer cell imaging study

Human monocytic/macrophage (THP-1) cell line was used to understand the fluorescence imaging potential of compounds **1** and **2** in presence of Hg^{2+} ion in these cancer cell lines. Before the bioimaging study, MTT assay was conducted to inspect the cytotoxicity of **1** and **2** to the THP-1 cell line (Figs. S17 and S18). The assay revealed the non-cytotoxic effect on the THP-1 cell at concentrations in the range 12.5 μM–200 μM and the viability of the cell was remained above 95%. Confocal fluorescence imaging study was conducted using the lowermost concentration of **1**–**2** (12.5 μM) with Hg^{2+}ion concentrations of (0.5 μM) at incubation time of 0.5 h. The CSLM imaging study of the cancer cell line with compounds **1**–**2** with Hg^{2+} ion showed remarkable enhancement in fluorescence intensity in the subcellular level (Figs. 12 and 13). We also observed that on nucleus staining using DAPI (Blue channel), compounds **1**, **2** showed effective accumulation inside the nucleus (Fig. 14). The imaging results showed remarkable potential of **1** and **2** as fluorescent imaging probes for the intracellular detection of sensitive metal ions.

2.2. BSA binding study

Compounds containing hydrazone moieties are well known to interact with several proteins and nucleic acids. Several such studies have been reported in recent years in which hydrazone derivatives and their metal complexes showed strong interaction with albumin proteins. Furthermore, the fact that the synthesized ferrocenyl-rhodamine hydrazone compounds **1** and **2** showed selective interaction with metal ions, has led to our interest in studying the interaction with BSA protein. Bovine serum albumins (BSA) are the most widely studied proteins due to their ability to transport a variety of endogenous and exogenous moieties such as steroids, drug molecules, metabolites and modulates their delivery to cells and is usually selected for protein binding studies [26]. Therefore, to understand the protein binding activities of the ferrocenyl compound, BSA was used to study the tryptophan emission-quenching experiment [27]. Generally, the fluorescence of BSA is caused by three intrinsic characteristics of the protein, namely tryptophan, tyrosine and phenylalanine. The majority of the intrinsic fluorescence of BSA is provided by the two tryptophan residues, (Trp 134, Trp 213) while the other amino acid residues contribute weakly. The fluorescence from the indole group in tryptophan is extremely sensitive to its surrounding environment and has been extensively used as a spectroscopic probe for the structural and conformational changes in the protein. Variation in the molecular environment in the vicinity of a fluorophore can be assessed by the changes in fluorescence spectra in the presence of a quencher which provide clues for the understanding of the binding phenomenon [28]. In the present study, the interaction of BSA with compounds **1** and **2** was studied by absorption and fluorescence spectroscopy measurement at room temperature. A fixed solution of BSA (2 μM) was titrated with various concentrations of the compound (0–55 μM) and the fluorescence spectra were recorded in the range of 300 nm–500 nm upon excitation at 285 nm. The effect of the compounds on the fluorescence emission spectrum of BSA is shown in Fig. 15 and Fig. 16. Indeed the fluorescence emission intensities of BSA at 335 nm showed remarkable decreasing trends with increasing concentration of the different ferrocenyl compounds **1** and **2**. UV–Visible spectra of BSA in buffer solution

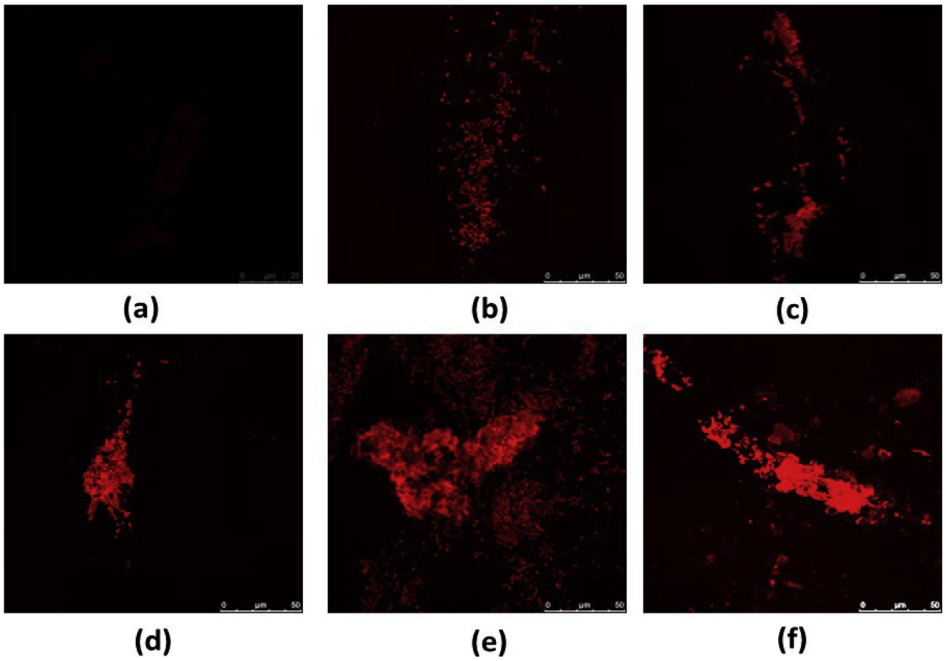

Fig. 11. CSLM imaging on *E.coli*, (a) Compound **1**, (b) **1** + 1 ppm Hg^{2+}, (c) **1** + 5 ppm Hg^{2+}, (d) **1** + 25 ppm Hg^{2+},(e) **1** + 50 ppm Hg^{2+}, (f) **1** + 100 ppm Hg^{2+}.

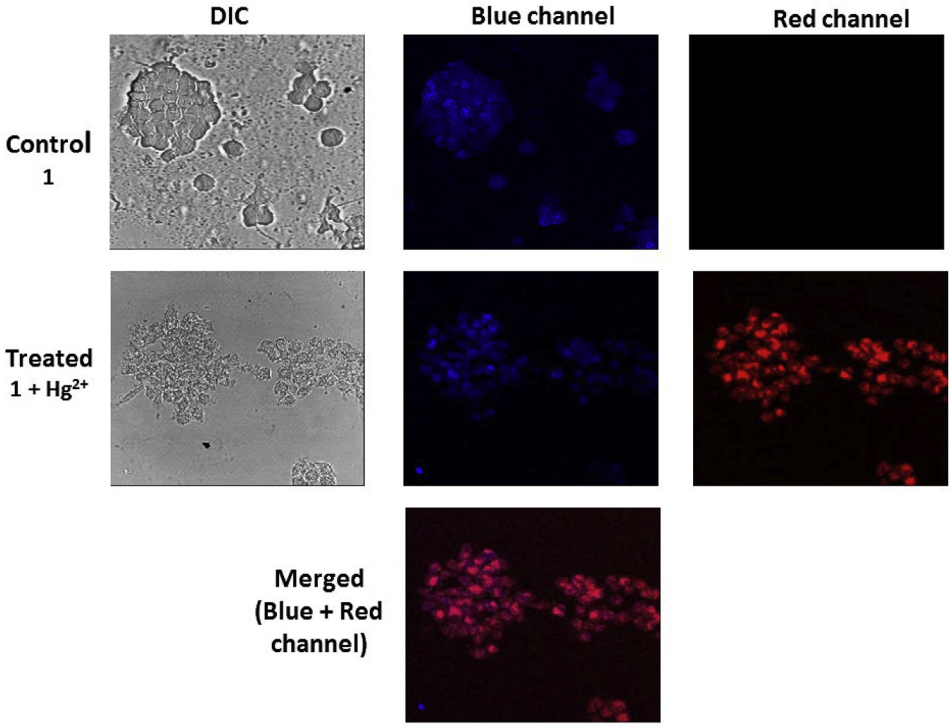

Fig. 12. Confocal fluorescence imaging of THP-1 cells in presence of compound **1** and Hg^{2+} (Blue channel: Nucleus staining with DAPI). (For interpretation of the references to color in this figure legend, the reader is referred to the Web version of this article.)

exhibits two absorption peaks in the ranges 200 nm−240 nm and 260 nm−300 nm which is considered to be characteristic backbone framework of the protein and it corresponds to the π−π* transition whereas the second peak at the higher wavelength region relates to the aromatic amino acids such as tryptophan (Trp), tyrosine (Tyr), and phenylalanine (Phe) and it corresponds to the n−π* transition [29b]. The absorption spectra of BSA was increased by increasing concentration of **1** and **2** with red shift which might be due to the change of the micro-environment around the peptide moieties of BSA caused by the interaction of the compounds. The interaction between compounds and water molecules induces the shielding of the peptide group from the aqueous environment and makes the energy of the π−π* transition lower, which leads to the bathochromic shift [29c,29d]. The spectral data indicates that the

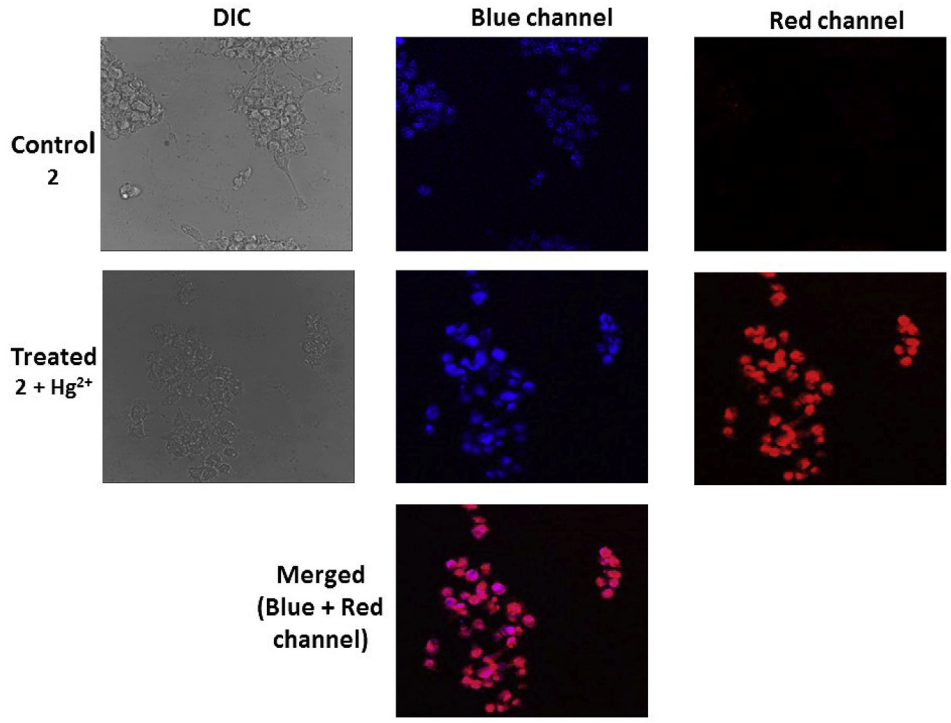

Fig. 13. Confocal fluorescence imaging of THP-1 cells in presence of compound **2** and Hg^{2+} (Blue channel: Nucleus staining with DAPI). (For interpretation of the references to color in this figure legend, the reader is referred to the Web version of this article.)

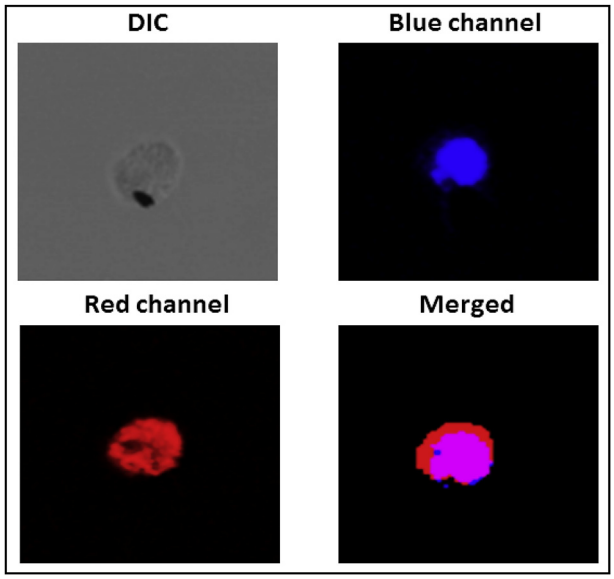

Fig. 14. Confocal fluorescence single cell imaging for compound **2** with Hg^{2+}.

interaction of the compound with BSA could cause conformational changes in protein structure, leading to changes in the tryptophan environment of BSA and suggested a definite interaction of the compound with the BSA protein.

Fluorescence quenching data were analyzed with the Stern-Volmer equation and Scatchard equation using corrected fluorescence data taking into account the effect of dilution. The Stern-Volmer quenching constant (K_{sv}) of the compounds have been calculated using the plot of I_0/I versus [Q], concentration, where I_0 and I are the emission intensity of BSA in the absence and in the presence of the quencher (equation (1)). The K_{sv} value obtained as a slope from the plot of I_0/I versus [Q] was found to be 4.11×10^5 and 4.94×10^5 for compounds **1** and **2** (Table 2).

$$I_0/I = 1 + K_{sv}[Q] \quad (1)$$

Proteins may interact with molecules using Vander Waals, electrostatic, hydrophobic and hydrogen bonding interactions. The observed quenching of fluorescence indicates some binding interactions between the compounds and suitable sites in the proteins. Binding of small molecules to a set of equivalent sites on a macromolecule can be understood by the Scatchard equation (equation (2)) [29a]. The binding constant and the number of binding sites (n) were obtained from the plot of $\log[(I_0-I)/I]$ vs. log [Q] and the values are shown in Table 2. The value of n is approximately equal to 1, indicating the presence of one binding site in BSA and follows 1:1 stoichiometric interaction between the compound and BSA protein [30].

$$\log[\mathbf{I_0}-I]/I = \log K_{\mathbf{b}} + n \log [Q] \quad (2)$$

In summary, we have explored the use of solid supported rice husk ash (RHA) for the facile synthesis of mono and selective functionalization of ferrocene to achieve rhodamine tagged hydrazone compounds. This organometallic system with fluorescent active rhodamine moiety showed selective heavy metal ion sensing property and effective molecular switching behavior. An unprecedented redox switching phenomenon was also observed on oxidation of the ferrocenyl center of compound **1** which led to an increase in the emission and absorption intensity. DFT calculation confirmed effective influence and interaction of the ferrocenyl organometallic fragment for the metal sensing and redox switching behavior. Confocal scanning laser microscopy study, performed using *E.coli* bacterial strain and THP-1 cell lines, revealed distinct uptake and sensing of heavy metal ion in the subcellular level with different concentration of compounds **1**, **2**.

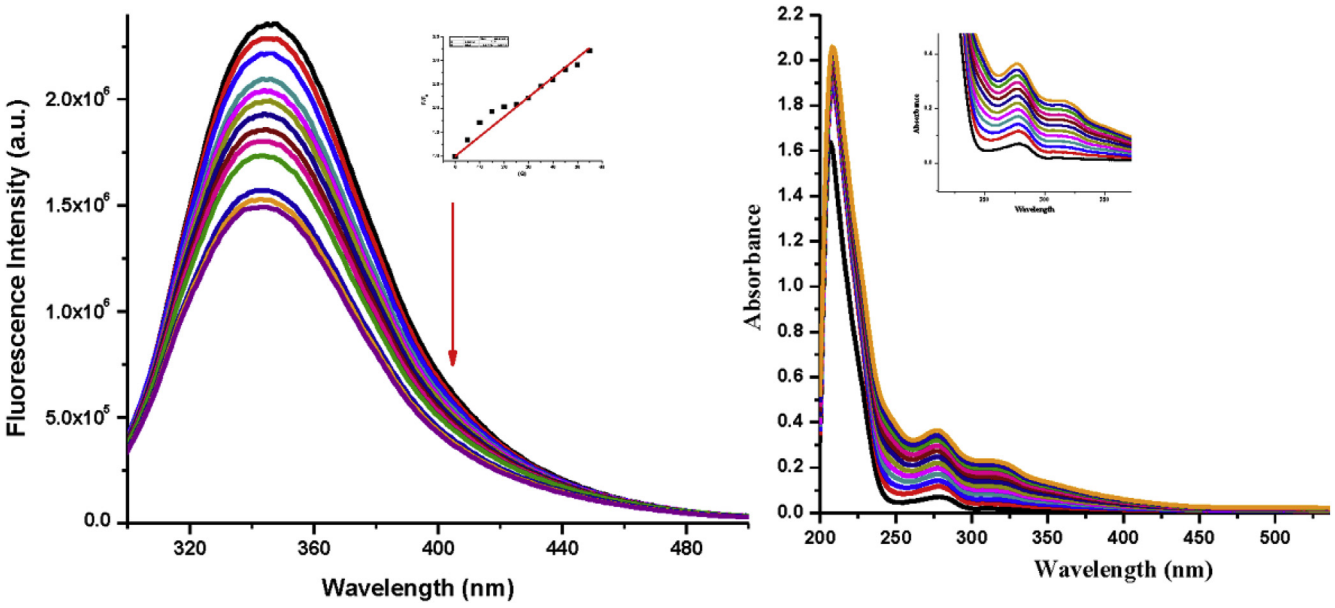

Fig. 15. Fluorescence emission and UV−Visible absorption spectra for BSA-**1** system (phosphate buffer, pH 7.2); Inset: Plot of F_0/F vs [Q], $R^2 = 0.991$. ($\lambda_{ex} = 285$ nm).

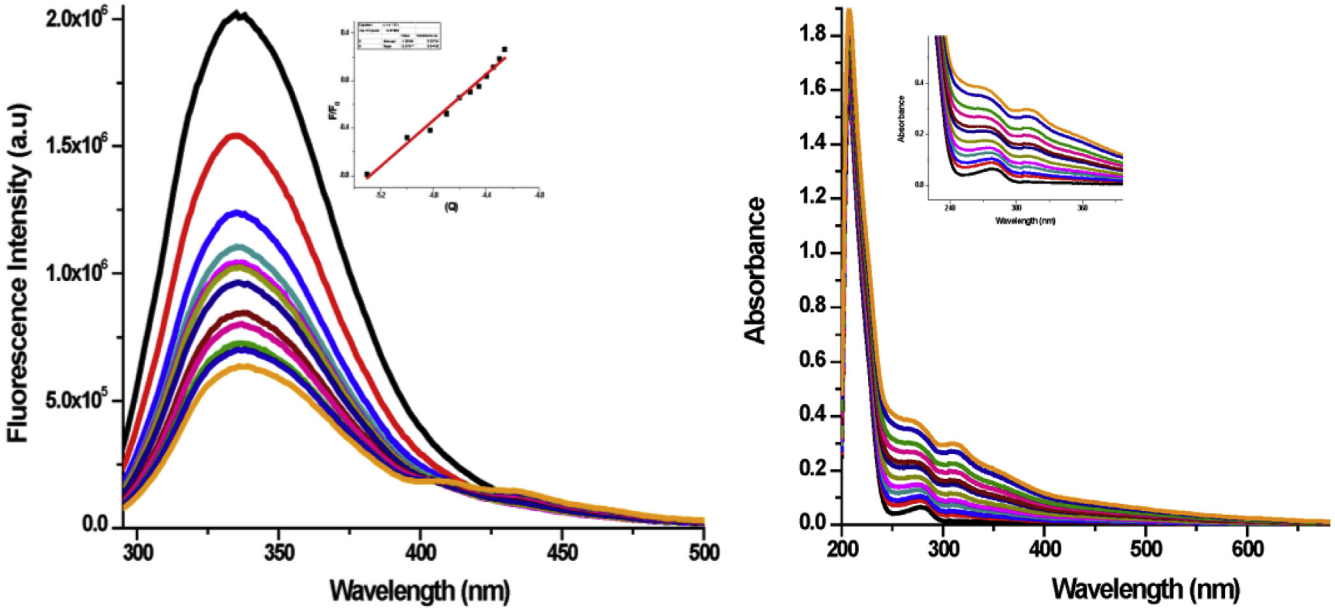

Fig. 16. Fluorescence emission and UV−Visible absorption spectra for BSA-**2** system (phosphate buffer, pH 7.2); Inset: Plot of F_0/F vs [Q]. ($\lambda_{ex} = 285$ nm).

Table 2
Quenching constant, binding constant and no. of binding sites for BSA with compounds **1** and **2**.

Compound	Quenching Constant K_{SV} [M^{-1}]	Binding Constant K_B	No: of binding sites (n)
1	4.11×10^5	2.02×10^5	1.0
2	4.94×10^5	3.2789×10^5	0.997

3. Experimental sections

3.1. General procedures

All reactions and manipulations were carried out under an inert atmosphere of dry, pre-purified argon using standard Schlenk line techniques. Solvents were purified, dried and distilled under argon atmosphere prior to use. Infrared spectra were recorded on a PerkinElmer Spectrum 2 spectrometer as KBr pellet or CH_2Cl_2 solution and NMR spectra on a 400 MHz Bruker spectrometer in $CDCl_3$ solvent. Elemental analyses were performed on a Vario El Cube analyser. Mass spectra were obtained on a SQ-300 MS instrument operating in ESI mode. UV spectroscopy was performed in Shimadzu 2700 in solution phase. Fluorescence spectroscopy was

recorded on Horiba Spectrophotometer 4000 in solution phase. TLC plates (20 × 20 cm, Silica gel 60 F254) were purchased from Merck. Imaging study was done by Confocal Scanning Laser Microscopy (CSLM) (Leica Microsystems, Hessen, Wetzlar, Germany). [(η^5-C_5H_4CHO)Fe((η^5-C_5H_5)], [Fe(η^5-$C_5H_4CHO)_2$], [(η^5-$C_5H_4COCH_3$) Fe(η^5-C_5H_5)], [Fe(η^5-$C_5H_4COCH_3)_2$], [H_2NN(H)C(O)R], (R = Rhodamine-6G) were prepared by following reported procedures [31–33].

3.2. Synthesis of [{(η^5-C_5H_5)Fe(η^5-C_5H_4)C(R)═NNC(O)-X}](R = CH_3 (1), H (2); X = Rhodamine-6G)

In a two neck round bottomed flask 1 gm of powdered Rice Husk Ash (RHA) was taken and Rhodamine-6G hydrazide (0.5 mmol) with monoacetyl ferrocene (0.5 mmol) or monoaldehyde ferrocene (0.5 mmol) was added. The mixture was stirred continuously for 8 h at room temperature for monoaldehyde ferrocene and at 60 °C for monoacetyl ferrocene. After the reaction, the solid mixture was extracted in dichloromethane solvent, filtered and dried in vacuum. The residue was then dissolved in dichloromethane and purified using column chromatography. Rapid elution with 25% ethylacetate:n-hexane solvent mixture afforded a pale orange colored compounds, [{(η^5-C_5H_5)Fe(η^5-C_5H_4)C(R)═NNC(O)-X}] (R = CH_3 (**1**), H (**2**); X = Rhodamine-6G). (Yields: **1**: 256 mg (80%); **2**: 288 mg (92%))

1 Anal. calcd. (found): C, 71.47 (71.62); H, 6.00 (5.89); N, 8.77 (8.65). IR (ν cm^{-1}, CH_2Cl_2): 1708 (s), 1637 (m), 1620 (vs), 1517 (vs). ^{1}H NMR (δ, $CDCl_3$): 1.32 (t, J = 7.2 Hz, 6H, -C*H*$_3$), 1.9 (s, 6H, -C*H*$_3$), 1.99 (s, 3H, -C*H*$_3$), 3.2 (q, J = 7.2 Hz, 4H, -C*H*$_2$), 3.6 (s, 2H, -N*H*), 3.60 (s, 5H, η^5-C_5H_5), 4.23 (t, J = 2 Hz, 2H, η^5-C_5H_4), 4.5 (t, J = 2 Hz, 2H, η^5-C_5H_4), 6.42 (d, 4H, -C_6H_2), 7.04 (t, 1H, -C_6H_4), 8.02 (m, 1H, -C_6H_4), 8.12 (s, 1H, *H*). ^{13}C NMR (δ, $CDCl_3$): 14.82 (-C*H*$_3$), 16.84(-C*H*$_2$C*H*$_3$), 18.51 (-C*H*$_3$), 38.40 (-*H*NC*H*$_2$-), 68.17 (η^5-C_5H_4), 68.21 (η^5-C_5H_4), 69.54 (η^5-C_5H_4), 70.21 (η^5-C_5H_4),81.63 (η^5-C_5H_4), 96.72 (Ar), 107.24 (Ar), 117.33 (Ar), 122.77 (Ar), 123.98 (Ar), 128.22 (Ar), 128.47 (Ar), 128.81 (Ar), 128.90 (Ar), 130.90 (Ar), 131.78 (Ar), 132.10 (Ar), 147.18 (Ar), 151.28 (Ar), 152.33 (Ar), 160.25 (-C═N), 1172.06 (-C═O). MS (ESI): m/z 639.56 $(M + 1)^+$.

2 Anal. calcd. (found): C, 71.15 (71.32); H, 5.81 (5.68); N, 8.97 (8.86). IR (ν cm^{-1}, CH_2Cl_2): 1683 (vs), 1637 (m), 1621 (vs), 1515 (vs). ^{1}HNMR (δ, $CDCl_3$): 1.3 (t, J = 7.2 Hz, 6H, C*H*$_3$), 1.9 (s, 6H, C*H*$_3$), 2.08 (s, 3H, C*H*$_3$), 2.23 (s, 3H, C*H*$_3$), 3.18 (q, J = 7.2 Hz, 4H, C*H*$_2$), 3.55 (s, 2H, -N*H*), 4.27 (t, 2H, η^5-C_5H_4), 4.29 (t, J = 2 Hz, 2H, η^5-C_5H_4), 4.49 (t, J = 2 Hz, 2H, η^5-C_5H_4), 4.61 (t, 2H, η^5-C_5H_4), 6.38 (s, 4H, C_6H_4), 7.15 (t, 1H, C_6H_4), 7.51 (m, 2H, C_6H_4), 7.96 (m, 1H, C_6H_4). ^{13}C NMR (δ, $CDCl_3$): 14.78 (-C*H*$_3$), 16.85 (-C*H*$_2$C*H*$_3$), 18.54 (-C*H*$_3$), 38.38 (-*H*NC*H*$_2$-), 69.68 (η^5-C_5H_4), 71.50 (η^5-C_5H_4), 71.99 (η^5-C_5H_4), 73.85 (η^5-C_5H_4), 80.34 (η^5-C_5H_4), 82.69 (η^5-C_5H_4), 81.15 (η^5-C_5H_4), 96.64 (Ar), 106.90 (Ar), 117.38 (Ar), 122.81 (Ar), 124.00 (Ar), 128.29 (Ar), 131.07 (Ar), 132.36 (Ar), 147.19 (Ar), 151.63 (Ar), 152.07 (Ar), 160.40 (Ar), 170.36 (-C═N), 202.61 (-C═O). MS (ESI): m/z 625.36 $(M + 1)^+$.

3.3. Bacterial culture and imaging

Bacterial strain was grown in 1 ml Luria Bertani (LB) broth (Himedia, India) and the bacterial culture was incubated for 24 h at 37 °C. Solution of compound **1** (10^{-5} M) was then added to the culture tube and incubated for 5 h at 37 °C. The bacterial culture was spread into a glass slide and dipped into the tube containing 5 ml LB medium for 1 h supplemented with different concentrations of Hg^{2+}(1 ppm–100 ppm). The slides were washed two times with phosphate buffer saline (PBS) and dried. Confocal Scanning Laser Microscopy (CSLM) (Leica Microsystems, Hessen, Wetzlar, Germany) was studied using the treated slides to observe the internal structure of the bacterial strain.

3.4. Cell culture, cytotoxicity assay and bioimaging studies

MTT assay was conducted to inspect the cytotoxicity of **1** and **2** to the THP-1 cell line before the bio-imaging study. 2.5×10^4 cells were seeded per well and PMA differentiated overnight for performing cell viability experiments. Next day after PMA wash, cells were treated with different concentration of **1**–**2** (12.5 μM-200 μM) and kept in incubation for 72 h. At the end of the treatment, 10 μl of MTT (5 mg/ml) was added to each well and incubated at 37 °C. After 2–3 h of incubation, OD was measured at 562 nm using microplate reader (PerkinElmer, USA). The percentage of viable cells was calculated according to the following formula:

% viability = OD of drug -treated sample/OD of untreated sample) *100

After 72 h of incubation time, the compound showed non-cytotoxic effect on the THP-1 cell even at higher concentration i.e. 200 μM. Viability of the cell remained above 95%. Therefore, the lowermost concentration of **1**–**2** (12.5 μM) has been used for imaging purpose. The ability of **1**–**2** to detect intracellular Hg^{2+} ions in human monocytic/macrophage (THP-1) cell line was then evaluated by fluorescent imaging studies. Differentiated THP-1 cells were grown overnight on glass cover slips at a density of 10^5 cells/ml in 24 well plate. Next day, cells were washed, treated with **1**–**2** (12.5 μM) and kept in incubator for 1 hour at 37 °C. Then, Hg^{2+} (0.5 μM) was added and incubated for 0.5 h for better interaction. The fixed cells were then treated with 1 μg/ml solution of 4′, 6-diamidino-2-phenylindole (DAPI) for nucleus staining and then washed the cells three times by 1 x PBS of 10 min duration. Confocal Scanning Laser Microscopy (CSLM) (Leica Microsystems, Hessen, Wetzlar, Germany) was used to study the treated cells with different incubation time period and observe the intracellular imaging.

3.5. BSA binding experiment

BSA protein binding study was performed by tryptophan fluorescence quenching experiments using a BSA stock solution of 0.01 M phosphate buffer of pH 7.2. The fluorescence titrations were performed at the fixed BSA concentration (2 μM). In the fluorescence quenching experiment, quenching of the tryptophan residues of BSA was done by keeping the concentration of the BSA constant while increasing the compound (quencher) concentration from 0 to 55 μM. The fluorescence spectra were recorded at an excitation wavelength of 285 nm and an emission wavelength of 335 nm after each addition of the compound. The excitation and emission slit widths and scan rates were maintained constant for all of the experiments. UV–Visible absorption experiment was performed by taking fixed concentration of BSA (2 μM) with increasing concentration of compounds. The absorption spectrum was recorded between 200 nm–400 nm wavelength range.

3.6. Computational study

DFT calculations was carried out using Gaussian 09 (Version: ES64L-G09RevE.01) with LANL2DZ basis set at B3LYP level of theory. Geometry optimization of compounds **1, 2** and **[1.Hg^{2+}], [2.Hg^{2+}]** were carried out in gas phase by density functional theory (DFT) at B3LYP level using LANL2DZ basis sets. The spectroscopic and electronic property of these complexes has been computed by

time dependent DFT (TD-DFT) calculation at the same B3LYP level in gaseous phase [34].

Acknowledgements

S.C. is grateful to the Council of Scientific and Industrial Research (CSIR), India, for research funding (No. 01(2948)/18/EMR-II). We are thankful to Mr. Saswata Chakravartty, Director, Soleil Oilex Pvt. Ltd., WB, India, for providing us with rice husk and rice hush ash for the reaction purposes.

Appendix A. Supplementary data

Supplementary data to this article can be found online at https://doi.org/10.1016/j.jorganchem.2019.120999.

References

[1] (a) V. Balzani, A. Credi, M. Venturi, Molecular Devices and Machines: A Journey into the Nano World, Wiley-VCH, Weinheim, Germany, 2003;
(b) J.M. Tour, Acc. Chem. Res. 33 (2000) 791;
(c) C.Y. Chen, M. Wang, J.Y. Li, N. Pootrakulchote, L. Alibabaei, C.H. Ngocle, J.D. Decoppet, J.H. Tsai, C. Gratzel, C.G. Wu, S.M. Zakeeruddin, M. Gratzel, ACS Nano 3 (2009) 3103;
(d) V. Balzani, A. Credi, F.M. Raymo, J.F. Stoddart, Angew. Chem. Int. Ed. 39 (2000) 3348;
(e) D.C. Magri, G.J. Brown, G.D. McClean, A.P. de Silva, J. Am. Chem. Soc. 128 (2006) 4950;
(f) F.M. Raymo, Adv. Mater. 14 (2002) 401;
(g) W. Skibar, H. Kopacka, K. Wurst, C. Salzmann, K.-H. Ongania, F.F. Biani, P. Zanello, B. Bildstein, Organometallics 23 (2004) 1024;
(h) S.A. Getty, C. Engtrakul, L. Wang, R. Liu, S.H. Ke, H.U. Baranger, W. Yang, M.S. Fuhrer, L.R. Sita, Phys. Rev. B 71 (2005) 1;
(i) P. Wan, Y. Jiang, Y. Wang, Z. Wang, X. Zhang, Chem. Commun. (2008) 5710;
(j) V.S. Miguel, C.G. Bochet, A. Del Campo, J. Am. Chem. Soc. 133 (2011) 5380;
(k) D.M. Lyons, J. Mohanraj, G. Accorsi, N. Armaroli, P.D.W. Boyd, New J. Chem. 35 (2011) 632;
(l) D. Pearson, A.J. Downard, A.M. Taylor, A.D. Abell, J. Am. Chem. Soc. 129 (2007) 14862;
(m) D. Gust, T.A. Moore, A.L. Moore, Chem. Commun. (2006) 1169;
(n) D. Roldan, V. Kaliginedi, S. Cobo, V. Kolivoska, C. Bucher, W. Hong, G. Royal, T. Wandlowski, J. Am. Chem. Soc. 135 (2013) 5974.

[2] (a) M. Irie, Chem. Rev. 100 (2000) 1683;
(b) C.C. Ko, V.W.W. Yam, J. Mater. Chem. 20 (2010) 2063;
(c) D.C. Magri, Engineering luminescent molecules with sensing and logic capabilities, in: E. Katz (Ed.), Molecular and Supramolecular Information Processing: from Molecular Switches to Logic Systems, Wiley-VCH Verlag, Weinheim, Germany, 2012, pp. 79–98;
(d) Y.L. Huang, A.S. Walker, E.W. Miller, J. Am. Chem. Soc. 137 (2015) 10767;
(e) Y. Hasegwa, T. Nakagawa, T. Kawai, Coord. Chem. Rev. 254 (2010) 2643;
(f) A. Nayak, H.W. Liu, G. Belfort, Angew. Chem. 45 (2006) 4094;
(g) L. Zang, R. Liu, M.W. Holman, K.T. Nguyen, D.M. Adams, J. Am. Chem. Soc. 124 (2002) 10640;
(h) G. Wang, J. Zhang, J. Photochem. Photobiol. 13 (2012) 299;
(i) J.L. Zhang, J.Q. Zhong, J.D. Lin, W. Ping, K. Wu, G. Qin, T.S. Andrew, W. Chen, Chem. Soc. Rev. 44 (2015) 2998;
(j) P.A. Liddell, G. Kodis, A.L. Moore, T.A. Moore, D. Gust, J. Am. Chem. Soc. 124 (2002) 7668;
(k) A.J.M. Huxley, M. Schroeder, H.Q. Nimal Gunaratne, A.P. De Silva, Angew. Chem. Int. Ed. 53 (2014) 3622;
(l) L. Wang, W. Lian, H. Yao, H. Liu, ACS Appl. Mater. Interfaces 7 (2015) 5168.

[3] (a) M. Li, Z. Guo, W. Zhu, F. Marken, T.D. James, Chem. Commun. 51 (2015) 1293;
(b) S.R. Bhatta, V. Bheemireddy, A. Thakur, Organometallics 36 (2017) 829;
(c) G.J. Scerri, M. Cini, J.S. Schembri, P.F. da Costa, A.D. Johnson, D.C. Magri, ChemPhysChem 18 (2017) 1742;
(d) D.C. Magri, A.D. Johnson, J.C. Spiteri, J. Fluoresc. 27 (2017) 551;
(e) R. Martínez, I. Ratera, A. Tárraga, P. Molina, J. Veciana, Chem. Commun. (2006) 3809;
(f) A. Chaubey, B.D. Malhotra, Biosens. Bioelectron. 17 (2002) 441;
(g) X. Wang, H. Gu, F. Yin, Y. Tu, Biosens. Bioelectron. 24 (2009) 1527;
(h) R. Pauliukaite, M.E. Ghica, O.F. Filho, C.M. A Brett, Electrochim. Acta 55 (2010) 6239;
(i) F. Kuralay, T. Vural, C. Bayram, E.B. Denkbas, S. Abaci, Colloids Surfaces B Biointerfaces 87 (2011) 18;
(j) R. Gracia, D. Mecerreyes, Polym. Chem. 4 (2013) 2206;
(k) R. Martínez, I. Ratera, A. Tárraga, P. Molina, J. Veciana, Chem. Commun. (2006) 3809;
(l) F. Zapata, A. Caballero, A. Espinosa, A. Tárraga, P. Molina, Dalton Trans. (2009) 3900;
(m) R. Zhang, Z. Wang, Y. Wu, H. Fu, J. Yao, Org. Lett. 10 (2008) 3065;
(n) H. Yang, Z. Zhou, K. Huang, M. Yu, F. Li, T. Yi, C. Huang, Org. Lett. 9 (2007) 4729.

[4] (a) J. Xiang, X. Pi, X. Chen, L. Xiang, M. Yang, H. Ren, X. Shen, N. Qi, C. Deng, Biosens. Bioelectron. 96 (2017) 268;
(b) C. Engtrakul, L.R. Sita, Nano Lett. 1 (2001) 541;
(c) R. Sakamoto, M. Murata, H. Nishihara, Angew. Chem. Int. Ed. 45 (2006) 4793;
(d) D.Y. Wu, W. Huang, Z.H. Lin, C.Y. Duan, C. He, S. Wu, D.H. Wang, Inorg. Chem. 47 (2008) 7190.

[5] (a) S.S. Braga, A.M.S. Silva, Organometallics 32 (2013) 5626;
(b) K.N. Tiwari, J.P. Monserrat, A. Hequet, C. Ganem-Elbaz, T. Cresteil, G. Jaouen, A. Vessières, E.A. Hillard, C. Jolivalta, Dalton Trans. 41 (2012) 6451;
(c) P. Perjési, K. Takács-Novák, Z. Rozmer, P. Sohár, R.E. Bozak, T.M. Allen, Cent. Eur. J. Chem. 10 (2012) 1500;
(d) S. Top, C. Thibaudeau, A. Vessières, E. Brulé, F. Le Bideau, J.M. Joerger, A. Edgar, J. Marrot, P. Herson, G. Jaouen, Organometallics 28 (2009) 1414;
(e) M. Patra, G. Gasser, Chembiochem 13 (2012) 1232;
(f) G. Gasser, N.M. Nolte, Curr. Opin. Chem. Biol. 16 (2012) 84;
(g) C.G. Hartinger, N.M. Nolte, P.J. Dyson, Organometallics 31 (2012) 5677;
(h) M. Patra, G. Gasser, M. Wenzel, K. Merz, J.E. Bandow, N.M. Nolte, Organometallics 31 (2012) 5760;
(i) A. Csámpai, G.I. Túrós, A. Györfi, P. Sohár, J. Organomet. Chem. 694 (2009) 3667;
(j) K. Kiss, A. Csámpai, P. Sohár, J. Organomet. Chem. 695 (2010) 1852;
(k) R. Prasath, P. Bhavana, S.W. Ng, E.R.T. Tiekink, J. Organomet. Chem. 726 (2013) 62;
(l) J. Quirante, F. Dubar, A. Gonzalez, C. Lopez, M. Cascante, R. Cortes, I. Forfar, B. Pradines, C. Biot, J. Organomet. Chem. 696 (2011) 1011;
(m) C. Policar, J.B. Waern, M.-A. Plamont, S. Clède, C. Mayet, R. Prazeres, J.-M. Ortega, A. Vessières, A. Dazzi, Angew. Chem. Int. Ed. 50 (2011) 860.

[6] (a) X. Chen, T. Pradhan, F. Wang, J.S. Kim, J. Yoon, Chem. Rev. 112 (2012) 1910;
(b) K.P. Carter, A.M. Young, A.E. Palmer, Chem. Rev. 114 (2014) 4564;
(c) G. Sivaraman, T. Anand, D. Chellappa, Analyst 137 (2012) 5881;
(d) K. Li, Y. Xiang, X. Li, R. Wang, A. Tong, B.Z. Tang, J. Am. Chem. Soc. 136 (2014) 1643;
(e) P. Mahato, S. Saha, E. Suresh, R.D. Liddo, P.P. Parnigotto, M.T. Conconi, M.K. Kesharwani, B. Ganguly, A. Das, Inorg. Chem. 51 (2012) 1769;
(f) Q. Huang, Q. Zhang, E. Wang, Y. Zhou, H. Qiao, L. Pang, Y. Fang, Spectrochim. Acta A 152 (2016) 70;
(g) K. Wechakorna, K. Suksenc, P. Piyachaturawatc, P. Kongsaeree, Sens. Actuators, B 228 (2016) 270;
(h) W. Huang, C. Song, C. He, G. Lv, X. Hu, X. Zhu, C. Duan, Inorg. Chem. 48 (2009) 5061.

[7] (a) S. Mishra, S. Dewangan, S. Giri, S.M. Mobin, S. Chatterjee, Eur. J. Inorg. Chem. (2016) 5485;
(b) V. Tirkey, S. Mishra, H.R. Dash, S. Das, B.P. Nayak, S.M. Mobin, S. Chatterjee, J. Organomet. Chem. 732 (2013) 122;
(c) S.K. Patel, V. Tirkey, S. Mishra, H.R. Dash, S. Das, M. Shukla, S. Saha, S.M. Mobin, S. Chatterjee, J. Organomet. Chem. 749 (2014) 75.

[8] S. Mishra, V. Tirkey, A. Ghosh, H.R. Dash, S. Das, M. Shukla, S. Saha, S.M. Mobin, S. Chatterjee, J. Mol. Struct. 1085 (2015) 162.

[9] (a) S. Dewangan, T. Barik, S. Mishra, S. Mawatwal, S. Kumari, S. Giri, S. Das, R. Dhiman, C. Wölper, S. Chatterjee, Appl. Organomet. Chem. 32 (2018) 4612;
(b) S. Dewangan, S. Mishra, S. Mawatwal, R. Dhiman, R. Parida, S. Giri, C. Wolper, S. Chatterjee, ChemistrySelect 4 (2019) 4434.

[10] (a) I.J. Schalk, O. Cunrath, Environ. Microbiol. 18 (2016) 3227;
(b) C.T. O'Loughlin, L.C. Miller, A. Siryaporn, K. Drescher, M.F. Semmelhack, B.L. Bassler, Proc. Natl. Acad. Sci. U. S. A. 110 (2013) 17981;
(c) K.J. Waldron, N.J. Robinson, Nat. Rev. Microbiol. 7 (2009) 25.

[11] (a) N. Mangwani, S. Kumari, S. Das, Biotechnol. Genet. Eng. Rev. 32 (2016) 43;
(b) J.J. Braymer, D.P. Giedroc, Curr. Opin. Chem. Biol. 19 (2014) 59;
(c) K.J. Waldron, J.C. Rutherford, D. Ford, N.J. Robinson, Nature 460 (2009) 823;
(d) A.J. Guerra, D.P. Giedroc, Arch. Biochem. Biophys. 519 (2012) 210;
(e) A.W. Foster, D. Osman, N.J. Robinson, J. Biol. Chem. 289 (2014) 28095.

[12] (a) C. Correnti, R.K. Strong, J. Biol. Chem. 287 (2012) 13524;
(b) S. Kumari, N. Mangwani, S. Das, Spectrochim. Acta A 173 (2017) 655;
(c) N. Mangwani, S.K. Shukla, S. Kumari, T.S. Rao, S. Das, J. Appl. Microbiol. 117 (2016) 1012;
(d) N. Mangwani, S.K. Shukla, S. Kumari, S. Das, T.S. Rao, RSC Adv. 6 (2016) 57540;
(e) N. Mangwani, S. Kumari, S. Das, J. Biotechnol. Genet. Eng. Rev. 32 (2016) 43.

[13] (a) A. Mudhoo, V.K. Garg, S. Wang, Environ. Chem. Lett. 10 (2012) 109;
(b) E.D. Weinberg, Biochim. Biophys. Acta 1790 (2009) 600;
(c) T.E. Kehl-Fie, E.P. Skaar, Curr. Opin. Chem. Biol. 14 (2010) 218.

[14] (a) C. Arivazhagan, R. Borthakur, S. Ghosh, Organometallics 34 (2015) 1147;
(b) Y. Fang, Y. Zhou, Q. Rui, C. Yao, Organometallics 34 (2015) 2962;
(c) K. Huang, H. Yang, Z. Zhou, M. Yu, F. Li, X. Gao, T. Yi, C. Huang, Org. Lett. 10 (2008) 2557;
(d) H. Yea, F. Gea, X.C. Chenb, Y. Li, H. Zhanga, B.X. Zhaoa, J.Y. Miao, Sens. Actuators, B 182 (2013) 273.

[15] (a) K. Tanaka, F. Toda, Chem. Rev. 100 (2000) 1025;
(b) H. Zhu, S. Ould-Chikh, H. Dong, I. Llorens, Y. Saih, D.H. Anjum,

J.L. Hazemann, J.M. Basset, ChemCatChem 7 (2015) 3332;
(c) J. Cleophax, M. Liagre, A. Loupy, A. Petit, Org. Process Res. Dev. 4 (2000) 498;
(d) F. Toda, Acc. Chem. Res. 28 (1995) 480;
(e) G.W.V. Cave, C.L. Raston, J.L. Scott, Chem. Commun. (2001) 2159;
(f) T.W. Elkins, H.E. Hagelin-Weaver, Appl. Catal., A 497 (2015) 96.
[16] (a) J. Xu, R.D. Armstrong, G. Shaw, N.F. Dummer, S.J. Freakley, S.H. Taylor, G.J. Hutchings, Catal. Today 270 (2016) 93;
(b) J.T. Grant, J.M. Venegas, W.P. McDermott, I. Hermans, Chem. Rev. 118 (2018) 2769;
(c) K. Tanaka, Solvent-free Organic Synthesis, vol. 7, Wiley-VCH, Weinheim, 2003, p. 612;
(d) J.G. Hernández, E. Juaristi, J. Org. Chem. 75 (2010) 7107;
(e) A. Rahman, S.B. Jonnalagadda, Catal. Lett. 123 (2008) 264;
(f) K.R. Kloetstra, H.V. Bekkum, Chem. Commun. 10 (1995) 1005;
(g) B.M. Choudary, M.L. Kantam, A. Rahman, Ch V.R. Reddy, J. Mol. Catal. 206 (2003) 145;
(h) S. Wada, H. Suzuki, Tetrahedron Lett. 44 (2003) 399;
(i) , in: S.M. Roberts (Ed.), Catalysts for Fine Chemicals Synthesis, Microporous and Mesoporous Solid Catalysts, vol. 4, Wiley-VCH, New York, 2006.
[17] (a) P. Serna, B.C. Gates, Acc. Chem. Res. 47 (2014) 2612;
(b) D. Hellwinkel, K. Göke, Synthesis 9 (1995) 1135;
(c) M.R. Detty, R.S. Eachus, J.A. Sinicropi, J.R. Lenhard, M. McMillan, A.M. Lauzafame, H.R. Luss, R. Young, J.E. Eilers, J. Org. Chem. 60 (1995) 1663.
[18] (a) E. Stankovic, S. Toma, R.V. Boxel, I. Asselberghs, A. Persoons, J. Organomet. Chem. 426 (2001) 637;
(b) D. Villemin, A. BenAlloum, Phosphorus, Sulfur, Silicon Relat. Elem. 79 (1993) 33;
(c) G. Cooke, H.M. Palmer, O. Schulz, Synthesis 11 (1995) 1415;
(d) E. Stankovic, P. Elecko, S. Toma, Chem. Pap. 50 (1996) 68;
(e) G. Cooke, O. Schulz, Synth. Commun. 26 (1996) 2549.
[19] A. Ghosh, T. Barik, S. Dewangan, P.K. Majhi, T. Sasamori, S.M. Mobin, S. Giri, S. Chatterjee, Appl. Organomet. Chem. 33 (2019) 4838.
[20] A. Ghosh, S. Mishra, S. Giri, S.M. Mobin, A. Bera, S. Chatterjee, Organometallics 37 (2018) 1999.
[21] S.L. Pan, K. Li, L.-L. Li, M.-Y. Li, L. Shi, Y.-H. Liu, X.-Q. Yu, Chem. Commun. 54 (2018) 4955.
[22] M. Malischewski, K. Seppelt, J. Sutter, F.W. Heinemann, B. Dittrich, K. Mayer, Angew. Chem. Int. Ed. 56 (2017) 13372.
[23] (a) K.J. Waldron, J.C. Rutherford, D. Ford, N.J. Robinson, Nature 460 (2009) 823;
(b) A.J. Guerra, D.P. Giedroc, Arch. Biochem. Biophys. 519 (2012) 210;
(c) A.W. Foster, D. Osman, N.J. Robinson, J. Biol. Chem. 289 (2014) 28095;
(d) C. Correnti, R.K. Strong, J. Biol. Chem. 287 (2012) 13524.
[24] (a) E.D. Weinberg, Biochim. Biophys. Acta 1790 (2009) 600;
(b) T.E. Kehl-Fie, E.P. Skaar, Curr. Opin. Chem. Biol. 14 (2010) 218.
[25] (a) L.D. Palmer, E.P. Skaar, Annu. Rev. Genet. 50 (2016) 67;
(b) P. Chandrangsu, C. Rensing, J.D. Helmann, Nat. Rev. Microbiol. 6 (2017) 338.
[26] (a) Z.G. Yasseen, J. Chem. Pharm. Res. 4 (2012) 3361;
(b) D.S. Raja, N. Bhuvanesh, S.P.K. Natarajan, Inorg. Chem. 50 (2011) 12852;
(c) T. Banerjee, S.K. Singh, N. Kishore, J. Phys. Chem. B 110 (2006) 24147.
[27] T.T. Xing, S.H. Zhan, Y.T. Li, Z.Y. Wu, C.W. Yan, J. Coord. Chem. 66 (2013) 3149.
[28] (a) S. Bi, D. Song, Y. Tian, X. Zhou, Z. Liu, H. Zhang, Spectrochim. Acta A 61 (2005) 629;
(b) J.R. Lakowicz, Principles of Fluorescence Spectroscopy, third ed., vol. 63, Springer Science, New York, 2003.
[29] (a) P. Banerjee, S. Ghosh, A. Sarkar, S.C. Bhattacharya, J. Lumin. 131 (2011) 316;
(b) M. Taha, B.S. Gupta, I. Khoiroh, M.-J. Lee, Macromolecules 44 (2011) 8575;
(c) B.S. Gupta, M. Tahab, M.J. Lee, RSC Adv. 4 (2014) 51111;
(d) X. Zhao, R. Liu, Z. Chi, Y. Teng, P. Qin, J. Phys. Chem. B 114 (2010) 5625.
[30] X.L. Han, F.F. Tian, Y.S. Ge, F.L. Jiang, L. Lai, D.W. Li, Q.L. Yu, J. Wang, C. Lin, Y. Liu, J. Photochem. Photobiol., B 109 (2012) 1.
[31] U.T. Mueller-Westerhoff, Z. Yang, G. Ingram, J. Organomet. Chem. 463 (1993) 163.
[32] M. Vogel, M. Rausch, H. Rosenberg, J. Org. Chem. 22 (1957) 1016.
[33] X.F. Yang, X.Q. Guo, Y.B. Zhao, Talanta 57 (2002) 883.
[34] (a) A.D. Beck, J. Chem. Phys. 98 (1993) 5648;
(b) A. Lee, W. Yang, R.G. Parr, Phys. Rev. B. 37 (1988) 785;
(c) F. Furche, R. Ahlrichs, J. Chem. Phys. 117 (2002) 7433;
(d) G. Scalmani, M.J. Frisch, B. Mennucci, J. Tomasi, R. Cammi, V. Barone, J. Chem. Phys. 124 (2006), 094107.